ESTIMATION OF ULTIMATE BEARING CAPACITY OF STRIP FOOTINGS ON COHESIVE-FRICTIONAL SOILS USING NON-LINEAR SHEAR STRENGTH MODEL

Pham Ngoc Quang*, Pham Ngoc Vinh

The University of Danang - University of Science and Technology, Vietnam

*Corresponding author: pnquang@dut.udn.vn

Abstract - This study widely investigated the applicability of the ultimate bearing capacity formula from the Architectural Institute of Japan (AIJ) while considering the effect of footing width. An in-house RPFEM program was developed using a non-linear shear strength model that is sensitive to confining stress. The research focuses on evaluating how footing width and soil properties affect the ultimate bearing capacity of strip footings. Coefficients within the AIJ formula were calculated and compared to those derived from the RPFEM, considering different combinations of cohesive and frictional soil strengths across various footing widths. The RPFEM results closely matched those obtained from the AIJ formula. This suggests that using a non-linear shear strength model can accurately estimate the ultimate bearing capacity of strip footings on cohesive-frictional soils, taking into account the footing width.

Key words - Rigid plasticity; Non-linear shear strength model; Ultimate bearing capacity; Strip footing; RPFEM.

1. Introduction

When designing a foundation, it is crucial to evaluate the ultimate bearing capacity of shallow foundations. While the ultimate bearing capacity has been studied extensively [1, 2], and simplified bearing capacity equations have been developed, these equations often overlook the impact of footing width. However, the Architectural Institute of Japan (AIJ) [3] suggests that bearing capacity equations for building foundations should consider footing width effects, especially since building foundations are generally larger than those used in civil engineering structures. These equations developed semi-experimentally with the bearing capacity factors N_q, N_c, and N_γ (as detailed in Table 1), have become widely used in Japan. The formula for ultimate bearing capacity is provided in Equation (1), and these equations have been successfully applied in a wide variety of designs. However, it should be noted that these equations are semi-empirical, and their accuracy is not clearly defined. Advancements in bearing capacity equations are crucial for achieving economical rationalization in design.

$$q = i_c \alpha c N_c + i_\gamma \gamma_1 \beta B \eta N_\gamma + i_q \gamma_2 D_f N_q \qquad (1)$$

where, α and β are shape coefficients for which α=1 and β=0.5 are suggested by De Beer [4]. Parameters of c (kPa), ϕ (deg), and γ_1, γ_2 (kN/m³) are cohesive strength, frictional strength and unit weight of soils, respectively. Coefficients i_c, i_γ, and i_q are inclination factors. The coefficient $\eta = \left(\dfrac{B}{B_o} \right)^{(-1/3)}$ is the size effect factor, in which, B_o=1 (m) is the reference value in the footing width B.

Table 1. Comparison of various simplified UBC formulas

Author	Bearing capacity factor		
	N_q	N_γ	N_c
Terzaghi [1]	$e^{\pi \tan \phi} \tan^2 \left(\dfrac{\pi}{4} + \dfrac{\phi}{2} \right)$	$(N_q + 3) \tan(1.34\phi)$	$(N_q - 1)/\tan\phi$
Meyerhof [2]	$e^{\pi \tan \phi} \tan^2 \left(\dfrac{\pi}{4} + \dfrac{\phi}{2} \right)$	$(N_q - 1) \tan(1.4\phi)$	$(N_q - 1)/\tan\phi$
AIJ [3]	$e^{\pi \tan \phi} \tan^2 \left(\dfrac{\pi}{4} + \dfrac{\phi}{2} \right)$	$(N_q - 1) \tan(1.4\phi)$	$(N_q - 1)/\tan\phi$

Incorporating the dependency of shear characteristics on confining stress, as reported by [5] and [6], into the analysis of bearing capacity yields results consistent with those obtained using the Architectural Institute of Japan's (AIJ) bearing capacity equations for sandy soils. This consistency is achieved when applying a non-linear shear strength model to Toyoura sand [7]. However, when cohesive strength c is added to the shear strength of cohesive-frictional soil, it can lead to complex, non-linear effects that raise doubts about the reliability of bearing capacity equations [5, 6]. Consequently, this non-linear interaction introduces uncertainty, suggesting that traditional bearing capacity equations may not be sufficient to estimate the bearing capacity of strip footing accurately. This study aims to estimate the ultimate bearing capacity of strip footing using the in-house RPFEM program code developed by the author [15 - 27]. The rigid plastic finite element method (RPFEM) has been successfully employed in geotechnical engineering, as evidenced by works such as those by [8 - 23]. In this study, the focus is on the influence of footing width on ultimate bearing capacity using plastic constitutive equations based on both higher-order (nonlinear) and Drucker-Prager (linear) yield functions, to examine the applicability of the AIJ bearing capacity equations for cohesive-frictional soils.

2. Rigid-plastic constitutive equation considering nonlinear shear strength

2.1. Constitutive equation incorporating nonlinear strength properties in rigid-plastic deformation

For the nonlinearity of soil strength concerning the confinement pressure, the higher-order yield function of Eq. (2) is introduced. Here, $I_1 = tr(\boldsymbol{\sigma})$ represents the first invariant of the stress tensor σ, and $J_2 = \dfrac{1}{2} \mathbf{s} : \mathbf{s}$ represents the second invariant of the deviatoric stress tensor s. Here,

n, a, and b are coefficients representing material properties, with tensile stress defined as positive.

$$f(\mathbf{\sigma}) = aI_1 + (J_2)^n - b = 0 \tag{2}$$

Eq. (2) possesses properties that correspond to the Mises criterion ($a = 0$) or the Drucker-Prager criterion ($n = 1/2$), depending on the setting of coefficients n and a.

The strain rate $\dot{\varepsilon}$ is expressed according to the related flow rule in Eq. (3). Here, λ is a coefficient representing the magnitude of the strain rate, $\dot{e} = \sqrt{\dot{\varepsilon}:\dot{\varepsilon}}$ is the equivalent strain rate, and $\mathbf{I}$ is the unit tensor.

$$\dot{\varepsilon} = \lambda \frac{\partial f(\mathbf{\sigma})}{\partial \mathbf{\sigma}} = \frac{\left(a\mathbf{I} + nJ_2^{n-1}\mathbf{s}\right)}{\sqrt{3a^2 + 2n^2\left(b - aI_1\right)^{(2-1/n)}}}\dot{e} \tag{3}$$

Here, the volumetric strain rate $\dot{\varepsilon}_v$ is related to the equivalent strain rate by Eq. (3) as follows.

$$\dot{\varepsilon}_v = tr\dot{\mathbf{\varepsilon}} = \frac{3a}{\sqrt{3a^2 + 2n^2\left(b - aI_1\right)^{(2-1/n)}}}\dot{e} \tag{4}$$

Therefore, the deviatoric stress $\mathbf{s}$ and the first invariant of stress I_1 are expressed as functions of the equivalent strain rate and the volumetric strain rate, as defined by the strain rate.

$$\mathbf{s} = \frac{1}{n}\left(\frac{9a^2}{2n^2}\left(\frac{\dot{e}}{\dot{\varepsilon}_v}\right)^2 - \frac{3a^2}{2n^2}\right)^{\left(\frac{1-n}{2n-1}\right)}\left(3a\frac{\dot{\mathbf{\varepsilon}}}{\dot{\varepsilon}_v} - a\mathbf{I}\right) \tag{5}$$

$$I_1 = \frac{b}{a} - \frac{1}{a}\left(\frac{9a^2}{2n^2}\left(\frac{\dot{e}}{\dot{\varepsilon}_v}\right)^2 - \frac{3a^2}{2n^2}\right)^{\frac{n}{2n-1}} \tag{6}$$

From the fact that the deviatoric stress $\mathbf{s}$ and the first invariant of stress I_1 are expressed as functions of the strain rate, the following constitutive relationship can be obtained.

$$\mathbf{\sigma} = \left[\frac{1}{n}\left(\frac{9a^2}{2n^2}\left(\frac{\dot{e}}{\dot{\varepsilon}_v}\right)^2 - \frac{3a^2}{2n^2}\right)^{\left(\frac{1-n}{2n-1}\right)}\left(3a\frac{\dot{\mathbf{\varepsilon}}}{\dot{\varepsilon}_v} - a\mathbf{I}\right)\right]$$
$$+ \frac{1}{3}\left[\frac{b}{a} - \frac{1}{a}\left(\frac{9a^2}{2n^2}\left(\frac{\dot{e}}{\dot{\varepsilon}_v}\right)^2 - \frac{3a^2}{2n^2}\right)^{\frac{n}{2n-1}}\right]\mathbf{I} \tag{7}$$

The rigid-plastic constitutive equation represents the unconstrained flow of the material; thus, the magnitude of the strain rate is indefinite. However, for the case of a nonlinear yield function ($n=1$) as shown in Figure 1, the stress is uniquely determined by the strain rate in Eq. (7). This uniqueness arises from the fact that the direction of strain rate determined by the orthogonality rule (dilatancy characteristic) varies with stress, leading to a unique determination of stress concerning strain rate. The dilatancy characteristic continuously changes the volumetric expansion properties with stress level, and in cases where only tensile stress is applied, simple (volumetric) expansion is represented without the occurrence of shear strain, facilitating a straightforward representation of detachment due to tensile failure. However, the constitutive equation (Eq. (7)) poses challenges in numerical analysis due to the asymmetry of the stiffness matrix, limiting its applicability.
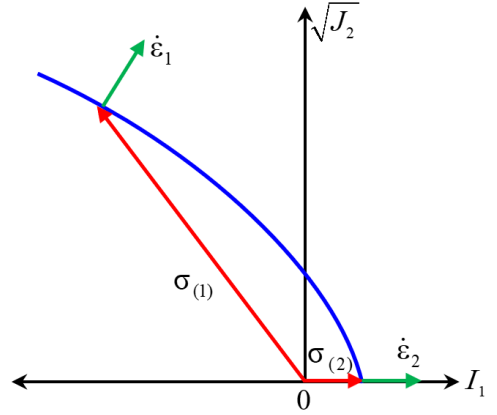
Figure 1. *Nonlinear yield function*

2.2. Explicit solution method for dilatancy characteristics

When aligning higher-order yield functions with the Drucker-Prager criterion ($n=0.5$), as depicted in Figure 2, there arises an issue where the yield surface exhibits a linear segment, leading to an indeterminate stress response concerning strain rate $\dot{\mathbf{\varepsilon}}$. Addressing this concern, Tamura [8, 9] clarified within rigid-plastic constitutive equations the existence of both determinate stresses (equivalent to Eq. (5)), which can be determined from material properties, and indeterminate stresses, which cannot be solely determined from material properties. They proposed employing constraint conditions for strain rate representing dilatancy characteristics (Eq. (8)) when utilizing the Drucker-Prager yield function. For notation simplicity, the coefficient ρ is introduced.

$$h(\dot{\mathbf{\varepsilon}}) = \dot{\varepsilon}_v - \frac{3a}{\sqrt{3a^2 + 2n^2\left(b - aI_1\right)^{(2-1/n)}}}\dot{e}$$
$$= \dot{\varepsilon}_v - \rho\dot{e} = 0 \tag{8}$$

The following equation represents a rigid-plastic constitutive equation for the Drucker-Prager yield function proposed by Hoshina *et al.* [24, 25]. It incorporates the constraint conditions for dilatancy characteristics (Eq. (8)) into the equation derived from substituting $n=1/2$ into Eq. (2) using the penalty method (where P is the penalty constant). Here, χ is the indeterminate multiplier of stress.

$$\mathbf{\sigma} = \frac{b}{\sqrt{3a^2 + 0.5}}\frac{\dot{\mathbf{\varepsilon}}}{\dot{e}} + \chi\frac{\partial h}{\partial \dot{\mathbf{\varepsilon}}} = \frac{b}{\sqrt{3a^2 + 0.5}}\frac{\dot{\mathbf{\varepsilon}}}{\dot{e}}$$
$$+ P\left(\dot{\varepsilon}_v - \rho\dot{e}\right)\left(\mathbf{I} - \frac{3a}{\sqrt{3a^2 + 0.5}}\frac{\dot{\mathbf{\varepsilon}}}{\dot{e}}\right) \tag{9}$$

The first term of the above equation represents the determinate stress according to the constitutive relationship, while the second term represents the stress component along the yield surface depicted in Figure 2, corresponding to the indeterminate stress. The indeterminate stress is

determined through force equilibrium equations when solving boundary value problems using the constitutive equation derived from Eq. (9).
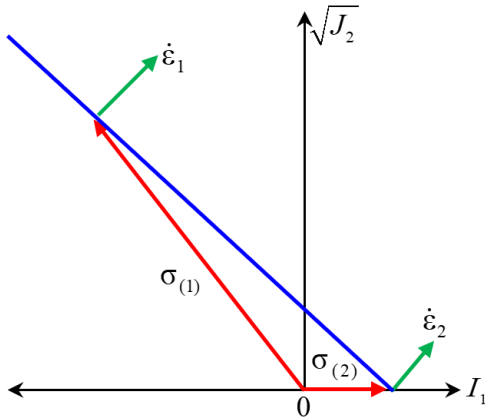
Figure 2. *Drucker-Prager (linear) yield function*

As mentioned earlier, due to the numerical challenges associated with Eq. (7), this study aimed to reconstruct the rigid-plastic constitutive equation using the formulation proposed by [24, 25]. The stress of the material is divided into determinate stress $\sigma^{(1)}$, which can be obtained solely from the yield function, and indeterminate stress $\sigma^{(2)}$, which cannot be determined solely. The determinate stress $\sigma_{(1)}$ is expressed using the associated flow rule as shown in Eq. (10), while the indeterminate stress $\sigma_{(2)}$ is expressed using the constraint conditions for dilatancy characteristics represented by Eq. (8) and an indefinite constant η, as shown in Eq. (11). Here, I_1 is a constant updated during the convergence calculation, which implies updating the Drucker-Prager criterion with each convergence calculation.

$$\boldsymbol{\sigma}^{(1)} = \xi \frac{\partial f(\boldsymbol{\sigma})}{\partial \boldsymbol{\sigma}} = \frac{\left(2nb + (1-2n)aI_1\right)}{\sqrt{3a^2 + 2n^2 \left(b - aI_1\right)^{(2-1/n)}}} \frac{\dot{\boldsymbol{\varepsilon}}}{\dot{e}} \qquad (10)$$

$$\boldsymbol{\sigma}^{(2)} = \eta \frac{\partial h(\dot{\boldsymbol{\varepsilon}})}{\partial \dot{\boldsymbol{\varepsilon}}} = \eta \left(\mathbf{I} - \frac{3a}{\sqrt{3a^2 + 2n^2 \left(b - aI_1\right)^{(2-1/n)}}} \right) \frac{\dot{\boldsymbol{\varepsilon}}}{\dot{e}} \quad (11)$$

From Eqs. (10) and (11), the rigid-plastic constitutive equation becomes the following Eq. (12). Furthermore, in this study, to accelerate the analysis speed, the constraint conditions for dilatancy characteristics (Eq. (8)) are incorporated into the constitutive equation as follows using the penalty method (where P is the penalty constant) [24, 25].

$$\boldsymbol{\sigma} = \frac{\left(aI_1 + 2n(b - aI_1)\right)}{\sqrt{3a^2 + 2n^2 \left(b - aI_1\right)^{(2-1/n)}}} \frac{\dot{\boldsymbol{\varepsilon}}}{\dot{e}}$$

$$+ P\left(\dot{\varepsilon}_v - \rho\dot{e}\right) \left(\mathbf{I} - \frac{3a}{\sqrt{3a^2 + 2n^2 \left(b - aI_1\right)^{(2-1/n)}}} \frac{\dot{\boldsymbol{\varepsilon}}}{\dot{e}} \right) \qquad (12)$$

The above equation allows for the explicit analysis of dilatancy characteristics, enabling stable calculations of displacement velocity fields even in highly nonlinear problems. Furthermore, Eq. (12) benefits from numerical analysis due to the symmetry of the stiffness matrix. The first invariant of stress is updated using the second

invariant of deviatoric stress, derived from transforming the yield function of Eq. (2), as follows.

$$I_1 = \frac{1}{a}\left(b - \left(J_2\right)^n\right) \qquad (13)$$

The rigid-plastic constitutive equation (Eq. (12)) is applicable to deforming bodies, thus presenting issues when applied to rigid bodies. In limit load analysis, where analysis including rigid body regions is necessary, the following rigid-plastic constitutive equation (Eq. (14)) is applied when the equivalent plastic strain rate $\dot{e}$ falls below the threshold $\dot{e}_o$.

$$\boldsymbol{\sigma} = \frac{\left(aI_1 + 2n(b - aI_1)\right)}{\sqrt{3a^2 + 2n^2 \left(b - aI_1\right)^{(2-1/n)}}} \frac{\dot{e}}{\dot{e}_o} \frac{\dot{\boldsymbol{\varepsilon}}}{\dot{e}}$$

$$+ P\left(\dot{\varepsilon}_v - \rho\dot{e}\right) \left(\mathbf{I} - \frac{3a}{\sqrt{3a^2 + 2n^2 \left(b - aI_1\right)^{(2-1/n)}}} \frac{\dot{e}}{\dot{e}_o} \frac{\dot{\boldsymbol{\varepsilon}}}{\dot{e}} \right) \qquad (14)$$

in case of $\dfrac{\dot{e}}{\dot{e}_o} < 1$

The replacement of the equivalent strain rate by a threshold value $\dot{e}_o$, as shown in the above equation, has the effect of discounting the shear strength of the ground by $\left(\dfrac{\dot{e}}{\dot{e}_o} < 1 \right)$. Similar to creating constitutive equations where the shear strength appears to decrease, allowing for a small strain rate $\dot{\boldsymbol{\varepsilon}}$ in rigid body portions prevents division by zero in Eq. (12) concerning stress within the yield function, thus enabling stable equilibrium equations to be solved. Regarding the setting of the threshold, numerical experiments with varying thresholds are conducted in advance, and in the numerical analysis examples in the paper, a value (10^{-10}) is used that does not affect the final results.

3. Effect of footing width on ultimate bearing capacity of a strip footing

3.1. Ultimate bearing capacity of strip footing under vertical load
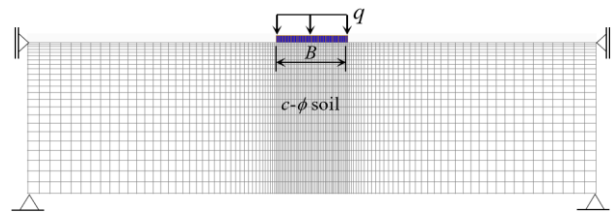
Figure 3. *Finite element model and boundary conditions of strip footing under uniform vertical load*

This study employs a two-dimensional model RPFEM to investigate the ultimate bearing capacity of strip footing under a uniform vertical load q. The load is applied along the strip footing with width B. This load factor q is defined as the ultimate bearing capacity (kPa) in plane strain conditions. Using a solid element, the strip footing is modeled with a large strength to simulate a rigid footing. Figure 3 illustrates the typical finite element mesh and boundary conditions utilized for RPFEM. Model dimensions

are carefully chosen to prevent the collapse load from influencing the development of the failure mechanism. In the model-building process, selecting the appropriate mesh size significantly enhances computed results and simulation accuracy. The number of initial and final meshes is determined iteratively by increasing the number of nodes and elements. Approximately 4000 final meshes are selected to ensure the reliability of the outcomes.

In RPFEM analysis, integrating nonlinear shear strength into bearing capacity assessments results in significant deviations from linear shear strength, particularly under low and high confining pressures, thereby exerting a substantial influence on evaluations of ultimate bearing capacity. This study aims to compare with the ultimate bearing capacity formula of the Architectural Institute of Japan (AIJ) by utilizing the reduction characteristics of internal friction angle concerning confining stress for Toyoura sand, creating a hypothetical ground with a frictional shear strength of ϕ=30°. While Table 2 presents the set ground constants, the study further conducted trial analyses by varying the cohesive strength c to extensively alter the shear strength characteristics of the hypothetical ground for comparative purposes. Throughout the analysis, the study varied the footing width to scrutinize the validity of the bearing capacity factor utilized in the formula concerning the cohesive strength c and the frictional strength ϕ.

Table 2. *Parameters for RPFEM analyses*

ϕ (°)	c (kPa)	Nonlinear material constants		
		a	b	n
30°	0	0.20	0.5	0.55
	10	0.21	9.8	0.55
	50	0.22	61.3	0.55
	100	0.24	129.5	0.55

Figure 4 illustrates the variation in bearing capacity when the footing width is varied as B=1, 5, 10, 30, 50, and 100 (m). The analysis results using the RPFEM based on the Drucker-Prager criterion (linear shear strength model) and the RPFEM based on the nonlinear yield function (nonlinear shear strength model), as well as the results based on [1, 2, 3] bearing capacity formulas, are compared. While there is some variability in the ultimate bearing capacity between the solution of Terzaghi [1], Meyerhof [2] and RPFEM (linear) due to the magnitude of cohesive strength, largely consistent results were obtained, whereas the ultimate bearing capacity obtained using the AIJ formula showed significant differences. Conversely, the ultimate bearing capacity evaluated by RPFEM (nonlinear), considering the confinement pressure dependency, showed relatively good agreement with the ultimate bearing capacity obtained by AIJ, regardless of the magnitude of cohesive strength c.

From the above observations, it can be concluded that the bearing capacity formula provided by the AIJ effectively captures the influence of nonlinear shear strength and is in good agreement with the RPFEM nonlinear model. In this investigation, while examining the effect of the cohesive strength c, it was found that despite some variability, the AIJ formula largely represents the ultimate bearing capacity accurately.

(a) *c*=0 kPa

(b) *c*=10 kPa

(c) *c*=50 kPa

(d) *c*=100 kPa
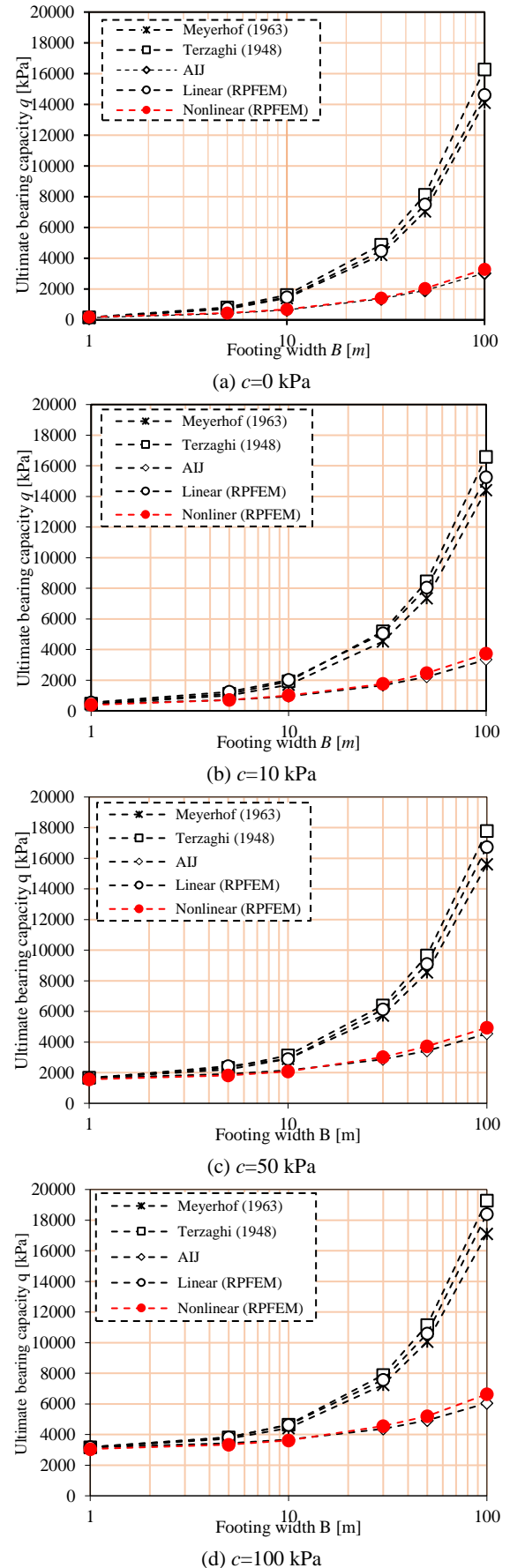
Figure 4. *Ultimate bearing capacity with non-linear shear strength in case of ϕ=30°*

3.2. Failure mechanism of strip footing under vertical load for linear and non-linear shear strength models

Figure 5 illustrates the failure mechanism of the ground at the limit state, computed by multiplying the arbitrary time increment by the velocity field obtained by RPFEM (linear and nonlinear models) for a footing width of B=10 (m). It is evident that the failure mechanism of the ground for both models appears similar. However, in the case of the linear shear strength model, the failure area is observed to be larger than that of the nonlinear shear strength model, particularly around the two footing edges. Additionally, the ultimate bearing capacity is generally obtained close to q=2034 kPa for the linear shear strength model and close to q=1080 kPa for the nonlinear shear strength model. This suggests that the results obtained using the nonlinear model property are reasonable and demonstrate that the effect of footing width on the ultimate bearing capacity can be accurately expressed by considering the nonlinear shear strength against the confining pressure [5].

(a) *Linear shear strength model (q=2034 kPa)*

(b) *Nonlinear shear strength model (q=1080 kPa)*
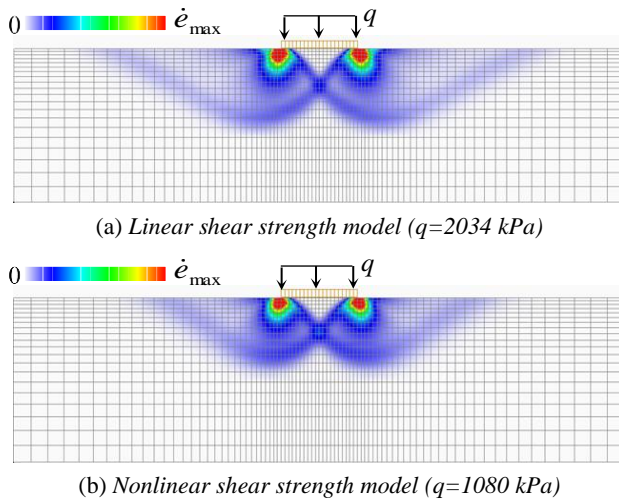
Figure 5. *Failure mechanism of strip footing, by using non-liner and linear shear strength model (B=10 m, ϕ=30º, c=10 kPa)*

3.3. Effect of cohesive strength c on failure mechanism of strip footing, using nonlinear shear strength model

For cohesive-frictional soil, the failure mechanism of the strip footing depends not only on the footing width B but also on soil properties such as cohesive strength c and internal friction angle ϕ. The question arises as to whether cohesive strength c affects the failure zone of the strip footing. Figure 6 shows the deformation diagrams of strip footing under uniform vertical load, using a nonlinear shear strength model. The deformation diagrams are presented for variations in the cohesive strength of the soil, with values of c=0 - 100 kPa. The strain rate distribution plot represents the predominant strain distribution at the limit state, which is believed to correspond to the displacement at the failure status. The results obtained in the figure are similar to the failure mode assumed by [28 - 30]. However, it is observed that as the cohesive strength c increases, the failure zone becomes larger. Since higher cohesive strength leads to greater ultimate bearing capacity of the foundation, the confining stress directly beneath the footing increases. It is understood that the influence of cohesive strength c

significantly affects the extent of the failure zone. Furthermore, the ultimate bearing capacities of the strip footing are typically observed to be q=682 kPa, 1080 kPa, 2041 kPa, and 3614 kPa for cohesive strengths of 0 kPa, 10 kPa, 50 kPa, 100 kPa, respectively. It is evident that as the cohesive strength c increases, the ultimate bearing capacity also increases.

(a) ϕ=30º - c=0 kPa (q=682 kPa)

(b) ϕ=30º - c=10 kPa (q=1080 kPa)

(c) ϕ=30º - c=50 kPa (q=2041 kPa)

(d) ϕ=30º - c=100 kPa (q=3614 kPa)
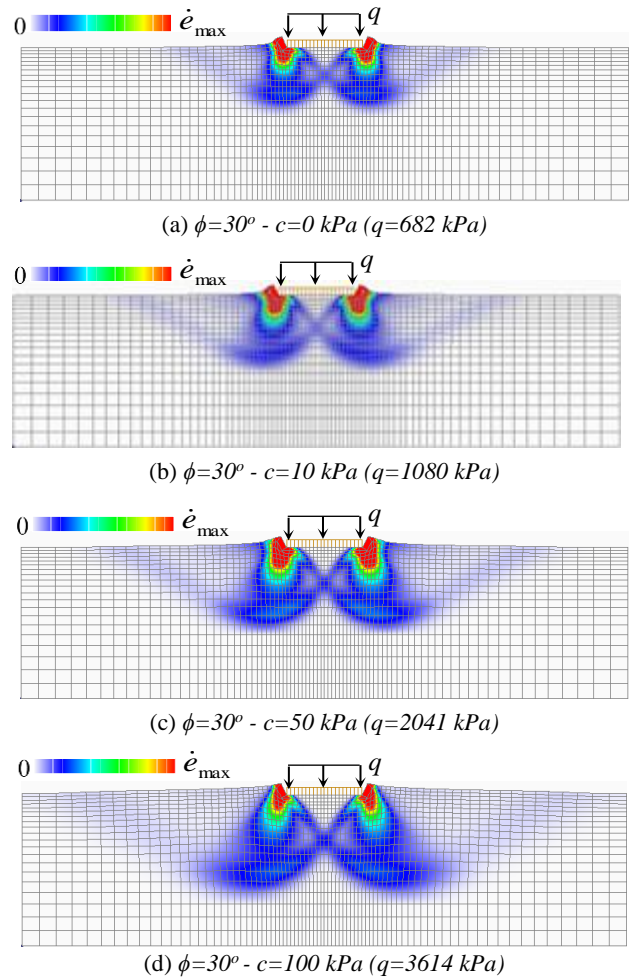
Figure 6. *Deformation diagrams of strip footing using nonlinear shear strength model (B=10 m)*

4. Conclusions

This study investigated the ultimate bearing capacity of a strip footing on cohesive-frictional soil, utilizing both linear and nonlinear shear strength models, in order to assess the AIJ bearing capacity formula. The impact of footing width and soil properties on the ultimate bearing capacity and failure mechanism was comprehensively analyzed.

Key conclusions drawn from the study are as follows:

(1) The study employed a rigid-plastic constitutive equation based on nonlinear yield functions to analyze ultimate bearing capacity. By incorporating the nonlinear strength characteristics of the ground affected by confining pressure, the RPFEM analysis results were consistent with those obtained using the AIJ bearing capacity formula, which considers the effects of footing width. Additionally, the investigation into the influence of cohesive strength on bearing capacity, alongside the friction angle, showed that

the AIJ bearing capacity formula exhibited satisfactory agreement with RPFEM analysis findings, thereby confirming its reliability.

(2) The comparison between linear and nonlinear shear strength models indicates that the nonlinear model better reflects the failure mechanism and ultimate bearing capacity of the strip footing, emphasizing the importance of considering nonlinear shear strength effects when analyzing the effect of footing width on bearing capacity.

(3) An increase in cohesive strength c, results in the extension of the failure zone of the strip footing. This phenomenon is attributed to the heightened ultimate bearing capacity associated with increased cohesion, consequently leading to elevated confining stress directly beneath the footing. Overall, it is evident that cohesive strength significantly influences the extent of the failure zone in the soil.

CRediT authorship contribution statement

Pham Ngoc Quang: Conceptualization, Methodology, Software, Validation, Investigation, Resources, Data curation, Writing - original draft, Visualization, Project administration, Funding acquisition. **Pham Ngoc Vinh:** Conceptualization, Software, Validation, Writing – review and editing.

REFERENCES

[1] K. Terzaghi, "Theoretical Soil Mechanics", Wiley, New York, 1948.

[2] G. G. Meyerhof, "Some recent research on the bearing capacity of foundations", *Canadian geotechnical journal* 1, pp.16-26, 1963.

[3] *Recommendations for design of building foundations*, Architectural Institute of Japan (AIJ), 2001.

[4] E. E. De Beer, "Bearing capacity and settlement of shallow foundations on sand", in *Proc. Symp. Bearing capacity and settlement of foundations*, 15-34, 1965.

[5] N. L. Du, S. Ohtsuka, T. Hoshina, and K. Isobe, "Discussion on size effect of footing in ultimate bearing capacity of sandy soil using rigid plastic finite element method", *Soils and foundations,* vol. 56, no. 1, 93-103, 2016.

[6] T. Iqbal, S. Ohtsuka, K. Isobe, Y. Fukumoto, and K. Kaneda, "Modified ultimate bearing capacity formula of strip footing on sandy soils considering strength non-linearity depending on stress level", *Soils and Foundations,* vol. 63, no. 3, 101325, 2023.

[7] F. Tatsuoka, M. Sakamoto, T. Kawamura, and S. Fukushima, "Strength and deformation characteristics of sand in plane strain compression at extremely low pressures", *Soils and Foundations*, vol 26, no. 1, pp. 65-84, 1986.

[8] T. Tamura, S. Kobayashi, and T. Sumi, "Limit analysis of soil structure by rigid plastic finite element method", *Soils and Foundations*, vol. 24, no. 1, pp.34-42, 1984.

[9] T. Tamura, S. Kobayashi, and T. Sumi, "Rigid-plastic finite element method for frictional materials", *Soils and Foundations*, vol. 27, no. 3, pp. 1-12, 1987.

[10] T. Tamura, "Rigid-plastic finite element method in geotechnical engineering", In *Computational Plasticity*. 1990.

[11] A. Asaoka, and S. Ohtsuka, "The analysis of failure of a normally consolidated clay foundation under embankment loading", *Soils and Foundations*, vol. 26, no. 2, pp. 47-59, 1986.

[12] A. Asaoka, and S. Ohtsuka, "Bearing capacity analysis of a normally consolidated clay foundation", *Soils and foundations*, vol. 27, no. 3, pp. 58-70, 1987.

[13] A. Asaoka, S. Ohtsuka, and M. Matsuo, "Coupling analyses of limiting equilibrium state for normally consolidated and lightly overconsolidated soils", *Soils and Foundations*, vol. 30, no. 3, pp. 109-123, 1990.

[14] S. Kobayashi, "Hybrid type rigid plastic finite element analysis for bearing capacity characteristics of surface uniform loading", *Soils and Foundations*, vol. 45, no. 2, pp. 17-27, 2005.

[15] P. N. Quang, S. Ohtsuka, K. Isobe, and Y. Fukumoto. "Group effect on ultimate lateral resistance of piles against uniform ground movement", *Soils and Foundations*, vol. 59, no. 1, pp. 27-40, 2019.

[16] P. N. Quang, S. Ohtsuka, K. Isobe, Y. Fukumoto, and T. Hoshina, "Ultimate bearing capacity of rigid footing under eccentric vertical load", *Soils and Foundations*, vol. 59, no. 6, pp. 1980-1991, 2019.

[17] P. N. Quang, S. Ohtsuka, K. Isobe, and Y. Fukumoto, "Limit load space of rigid footing under eccentrically inclined load", *Soils and Foundations*, vol. 60, no. 4, pp. 811-824, 2020.

[18] P. N. Quang, and S. Ohtsuka, "Ultimate bearing capacity of rigid footing on two-layered soils of sand–clay", *International Journal of Geomechanics*, vol. 21, no. 7, 04021115, 2021.

[19] P. N. Quang, S. Ohtsuka, K. Isobe, and Y. Fukumoto, "Consideration on Limit Load Space of Footing on Various Soils Under Eccentric Vertical Load", In *Challenges and Innovations in Geomechanics: Proceedings of the 16th International Conference of IACMAG-Volume 2 16*, 2021, pp. 75-84.

[20] P. N. Quang, S. Ohtsuka, K. Isobe, and Y. Fukumoto, "Limit load space of rigid strip footing on cohesive-frictional soil subjected to eccentrically inclined loads", *Computers and Geotechnics*, vol. 151, 104956, 2022.

[21] P. N. Quang, and S. Ohtsuka, "Numerical Investigation on Bearing Capacity of Rigid Footing on Sandy Soils Under Eccentrically Inclined Load", In *Proceedings of the 2nd Vietnam Symposium on Advances in Offshore Engineering: Sustainable Energy and Marine Planning*. Springer Singapore, 2022, pp. 333-341.

[22] P. N. Quang, S. Ohtsuka, K. Isobe, N.V. Pham, and P.H. Hoang, "Limit load space of rigid strip footing on sand slope subjected to combined eccentric and inclined loading", *Computers and Geotechnics*, vol. 162, 105652, 2023.

[23] P. N. Quang, S. Ohtsuka, K. Isobe, and P.H. Hoang, "Ultimate bearing capacity of rigid strip footings on c-ϕ soil subjected to combined eccentric and inclined loading", *in IOP Conference Series: Materials Science and Engineering*, vol. 1289, no. 1, p. 012088. IOP Publishing, 2023.

[24] T. Hoshina, "Rigid plastic stability analysis for slope including thin weak layer", *Japanese Geotechnical Journal*, vol. 6, no. 2, pp. 191-200, 2011.

[25] T. Hoshina, S. Ohtsuka, and K. Isobe, "Ultimate bearing capacity of ground by Rigid plastic finite element method taking account of stress dependent non-linear strength property", *Journal of Applied Mechanics*, vol. 6, no. 2, pp. I_327-I_336, 2012.

[26] P. N. Vinh, P. N. Quang, and H. Thang, "Effect of foundation surface roughness on ultimate bearing capacity of an eccentrically loaded foundation", *the University of Danang - Journal of Science and Technology*, vol 21, no. 12.1, pp. 28–33, 2023.

[27] P. N. Quang and P. N. Vinh, "Effect of footing roughness on ultimate bearing capacity of rigid strip footing on sandy soil slope", *the University of Danang - Journal of Science and Technology*, vol. 21, no. 12.1, pp. 22–27, 2023.

[28] D. Loukidis, T. Chakraborty, and R. Salgado, "Bearing capacity of strip footings on purely frictional soil under eccentric and inclined loads", *Canadian Geotechnical Journal*, vol. 45, no. 6, 768-787, 2008.

[29] A. Guetari, S. Benmebarek, and R.M Saddek, "Effect of the eccentric load on the bearing capacity of a strip footing founded on sand", *J. Appl.Eng. Sci. Technol.* vol. 4, no. 2, pp. 171-176, 2018.

[30] P. N. Quang, "*Estimation of Ultimate Lateral Resistance of Pile Group, and Ultimate Bearing Capacity of Rigid Footing under Complex Load by using Rigid Plastic Finite Element Method*", Doctoral dissertation, Nagaoka University of Technology, 2020.